# Direct 4D Slice-wise Whole-body Parametric PET Image Reconstruction for Continuous Bed Motion Acquisitions

Nicolas A. Karakatsanis, *Member, IEEE*, Abolfazl Mehranian, Michael E. Casey, and Habib Zaidi, *Senior Member, IEEE*

***Abstract*** **–Whole-body (WB) parametric PET imaging has recently demonstrated its clinical potential in enhancing quantification by employing robust dynamic analysis on a series of fast WB passes obtained either with step-and-shoot (SS) or continuous bed motion (CBM) acquisition mode. In particular, the CBM method has been associated with enhanced lesion detectability over SS in bed overlap regions for indirect Patlak influx rate constant ($K_i$) images. However, indirect Patlak is not very robust to the high noise levels often encountered in clinical WB dynamic PET imaging, thus limiting its clinical adoption. In addition, the CBM data at each transaxial slice are acquired within different time frames, while the SS data from all slices of a bed can be assigned a single average scan time. Thus, in the absence of list-mode data, accurate time data management may be challenging for dynamic CBM data analysis. In this study, we introduce a novel direct 4D WB parametric PET sinogram-based ordered subsets expectation maximization (OSEM) reconstruction algorithm specifically designed for the robust generalized Patlak analysis of dynamic CBM clinical PET data. The 4D algorithm employs the optimization transfer method to nest multiple faster Patlak subiterations within each of the slower global iteration steps and, thus, accelerate the convergence rate. Furthermore, an average scan time is assigned to each transaxial slice to construct an accurate set of slice-dependent nested Patlak model matrices and therefore permit a highly quantitative and efficient slice-wise 4D reconstruction of the CBM data. The clinical evaluation of the 4D CBM versus the 4D SS method was performed on a WB dynamic (12 passes) 18F-FDG PET/CT clinical study by switching the two modes between the passes. The quantitative analysis of a suspected high uptake foci located in a bed overlap region indicated an increase of 40-50% in $K_i$ target values and 35-45% in $K_i$ target-to-background scores for the CBM 4D Patlak method**

## I. Introduction

WHOLE-BODY (WB) imaging can be crucial in Positron Emission Tomography (PET) for the clinical evaluation of potentially metastatic tumors across the subject body in oncology studies. However, current commercial PET systems only support limited axial field-of-views (FOVs) and thus employ bed motion to enable acquisitions at multiple axial locations, known as bed positions, until the desired axial FOV is completely covered [1-4].

Furthermore, dynamic PET protocols have been recently expanded to WB FOVs to facilitate the clinical translation of the highly quantitative parametric PET imaging in clinical oncology [5,6]. The current advent of Time-of-Flight (TOF) and model-based resolution recovery reconstruction [7-9], permitted the reduction of scan time per bed thus enabling multiple faster WB PET passes for the same time and paving the way for WB dynamic PET acquisitions for enhanced quantification [10-13]. Nevertheless, such protocols typically involve a high number of bed motions thus compromising patient comfort and increasing the percentage of unused time, as data acquisition is interrupted during bed transitions [14].

The two bed motion mechanisms introduced so far in clinical PET systems are the step-and-shoot (SS) and the continuous bed motion (CBM) technologies. The SS scan mode has been established as the standard method to acquire WB PET data with limited axial FOV scanners, because it facilitates a simple synchronization of the discrete bed positions with the data acquisition [15-17]. Nevertheless, it results in non-uniform axial 3D PET sensitivity profiles, which may degrade image quality at the transaxial slices at the edges of each bed position, even after partial bed overlapping [18-21]. In addition, the elevated noise at the bed edges may propagate to the WB parametric images, thus further degrading their quantitative value.

On the contrary, the CBM mode employs a continuous bed motion during acquisition and thus enables a uniform sensitivity profile across all transaxial slices [22-30]. This feature may lead to lower noise propagation and better quantification regardless of the slice location [31-35], which may be particularly important for the faster acquisitions involved in WB PET and parametric images [36].

Nevertheless, indirect WB parametric imaging is applied on dynamic PET images that are often highly noisy, as each image is reconstructed from a single dynamic PET frame [5]. Consequently, the high noise levels can be propagated to the parametric images, regardless of the scan mode [6,36]. On the contrary, 4D parametric imaging involves the direct reconstruction of the parameters from the complete dynamic PET dataset, thus more efficiently utilizing all acquired data and limiting propagation of high noise levels in the parametric

This work was supported by the Swiss National Science Foundation under Grant SNSF 31003A-149957, the Swiss Cancer Research Foundation Grant KFS-3855-02-2016 and by Siemens Medical Solutions.

N. A. Karakatsanis (e-mail: nikolaos.karakatsanis@unige.ch) and H. Zaidi are with the Division of Nuclear Medicine and Molecular Imaging, Geneva University Hospital, Geneva, Switzerland

N. A. Karakatsanis is also with the Translational and Molecular Imaging Institute, Icahn School of Medicine at Mount Sinai, New York, NY, USA

A. Mehranian is with the Department of Biomedical Engineering, King's College London, London, UK

M. E. Casey is with Siemens Medical Solutions, Knoxville, TN, USA

H. Zaidi is also with Geneva Neuroscience Centre, University of Geneva, Geneva, Switzerland

H. Zaidi is also with the Department of Nuclear Medicine and Molecular Imaging, University of Groningen, Groningen, Netherlands

978-1-5090-1642-6/16/$31.00 ©2016 IEEE

images [37-40]. Moreover, the employment of either the robust standard Patlak (sPatlak) or more quantitative generalized Patlak (gPatlak) graphical analysis methods is recommended [41-44]. They both have previously demonstrated their clinical feasibility and high robustness to noise, particularly when used for the direct estimation of tracer influx rate constant ($K_i$) WB images [38-40].

However, the accuracy in the management of the scan time information of the 4D PET data may be more challenging for CBM than SS protocols In CBM mode, the 4D PET data are acquired while the bed is moving and, therefore, every transaxial slice should be assigned a different average scan time. On the other hand, all SS data of a bed position are acquired within the same time frame and thus an average scan time per bed position is sufficient. Moreover, the time handling per slice can be more complex for the 4D reconstruction as the scan time may affect the kinetic modeling components of the system matrix.

In this study, we propose a novel direct 4D ordered subsets expectation maximization (OS-EM) WB parametric PET image reconstruction algorithm specifically designed for CBM data. The concept of optimization transfer is employed to define surrogate objective functions to enable the nesting of multiple faster image-based generalized Patlak EM iterations within each slower tomographic global iteration cycle and thus accelerate the EM convergence rate [38,40,45-47]. Furthermore, the average scan time information per transaxial slice position is utilized to construct an accurate set of slice-dependent nested Patlak model matrices, that are decoupled from the tomographic system matrix, and therefore permit the efficient slice-wise 4D reconstruction of the CBM PET data.

## II. Methods and Materials

### A. PET sensitivity & time profiles for SS and CBM modes

In the SS mode, the bed is moving in discrete steps along certain axial positions, where it remains stationary during the PET acquisition. After the completion of the scan, the bed is translated to the next axial position to continue with the data acquisition. However the 3D PET sensitivity in stationary PET acquisitions can be significantly lower close to the edges of the axial FOV compared to the center. Therefore, the technique of bed positions partial overlapping was introduced to compensate for the significant non-uniformity in the axial sensitivity profile [1]. In particular, the SS data at each bed position are first reconstructed independently and the resulting images are averaged at the overlapping slices after applying weights to account for the relative sensitivity between the two beds. Nevertheless, considerably high noise levels and noise-induced bias at the bed edges may be propagated to the PET images, as the data overlapping process is conducted on the image space [5].

On the other hand, the CBM scan mode involves the uninterrupted acquisition of PET data over a selected axial range, while the bed is moving continuously and smoothly for a range of speeds and transaxial slices [22]. This concept has only recently been adopted in the clinic with the advent of Siemens Biograph Flow$^{TM}$ mCT PET/CT clinical system and offers significantly more flexibility and larger optimization margins when designing scan protocols [35,48]. In addition, the smooth bed motion without acquisition pauses is expected to limit any subject discomfort or data loss, relative to the SS mode, when many bed transitions are involved, such as with WB dynamic PET protocols [36]. Furthermore, with CBM mode each transaxial slice of the imaging subject is exposed to the same number of PET coincident line of responses (LORs), if the bed motion range is sufficiently long, thus resulting in a uniform axial sensitivity profile across the entire axial FOV except its two edges.

Fig. 1 synchronizes the temporal sequence of a WB PET acquisition across two bed positions between the two scan modes to illustrate the major differences in timing between SS and CBM WB PET scans. In addition, Fig. 2 presents the effect of the two scan modes on the 3D PET sensitivity axial profile. In fact, CBM mode may be viewed as the final evolution product of an SS scan process involving a gradually increasing number of bed positions along a given axial FOV.

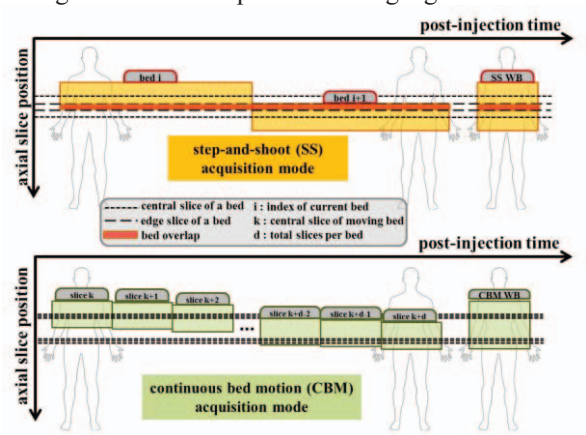


Fig. 1: Description of the temporal synchronization between the time sequence of acquisition and bed motion for the SS and CBM scan modes involving in this example two bed positions.

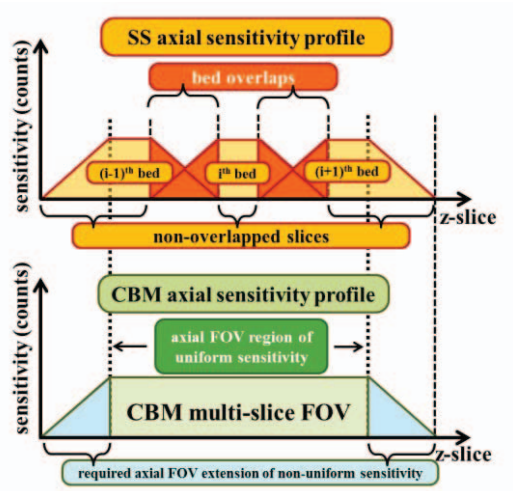


Fig. 2: 3D PET axial sensitivity profiles for the SS (top) and the CBM (bottom) WB acquisition modes involving in this example 3 bed positions.

Although each transaxial slice of a bed position in SS mode is associated with a different sensitivity, the bed remains stationary and thus the respective time sensitivity for that slice

is constant throughout the bed acquisition. If the slice position belongs to a bed overlap region, then the previous time profile will be extended to the new bed time frame with the same or different constant sensitivity value. On the contrary, the sensitivity time profiles in CBM mode are the same for all transaxial slices, except in the two edges of the axial FOV, but shifted in time depending on the axial location of each slice and the bed speed (Fig. 3).

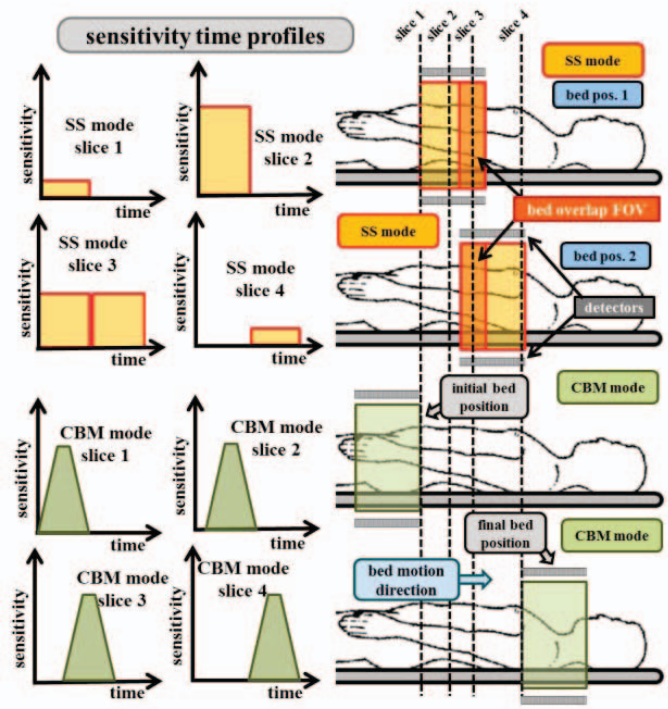


Fig. 3: 3D PET sensitivity time profiles (left) for SS and CBM modes over four characteristic transaxial slices (dotted lines). Two instances of bed motion are presented, corresponding to the start and end bed position.

### B. Direct 4D slice-wise Patlak from dynamic CBM PET

Our proposed direct 4D Patlak reconstruction algorithm employs the optimization transfer theory to define surrogate objective functions at each global tomographic iteration step and nest a Patlak OS-EM iterative loop to estimate the $K_i$ images with accelerated convergence rate [38],[40]. Moreover, as the Patlak reconstruction is conducted on the image space, it allows for the efficient use of the highly accurate CBM time $t_i$ in the Patlak model matrices $\boldsymbol{B}_i$ for each slice $i$, thus avoiding potential time approximations:

$$m_{i,jk}^{new} = \frac{m_{i,jk}^{old}}{\sum_n \boldsymbol{B}_{i,nk}} \sum_n \boldsymbol{B}_{i,nk} \left[ \frac{x_{j,new}^{n}}{\sum_k \boldsymbol{B}_{i,nk} m_{i,jk}^{old}} \right], \tag{1a}$$

$$\boldsymbol{B}_{i,nk} = \begin{bmatrix} \int_0^{t_{i,1}} C_P(t')dt' & C_P(t_{i,1}) \\ \vdots & \vdots \\ \int_0^{t_{i,n}} C_P(t')dt' & C_P(t_{i,n}) \end{bmatrix} \tag{1b}$$

where $m_{i,jk}$ is the $k$th parameter ($k$=2 parameters for sPatlak, including $K_i$) value in voxel $j$ at slice $i$, $n$ is the number of WB passes, $x_j^n$ is the respective dynamic PET estimate and $C_P(t_i)$ is the input function data.

The same framework (eq. 1a) is also applicable for gPatlak graphical analysis where the Patlak model matrices $\boldsymbol{B}_i$ have now a different internal form and an additional parameter, denoting the net tracer efflux rate ($k_{loss}$), needs to be also estimated [38,40]. However, in this study we limit our evaluation to the $K_i$ metric only as this parameter is associated with the most clinical interest in oncology studies.

### C. 4D CBM vs. SS Patlak in dynamic WB PET imaging

The proposed direct 4D CBM Patlak algorithm is evaluated versus the respective 4D SS algorithm employing data from the same human subject, as acquired with a dynamic WB PET/CT protocol on the Siemens Biograph Flow™ mCT scanner [9,35]. After a short 6-min dynamic cardiac PET scan to obtain the initial peak of the input function, 12 fast WB passes were acquired, half of which in SS and half in CBM mode [5]. The two modes were alternated successively to allow their balanced time interleaving and thus minimize the time differences between them for objective comparative evaluations [36]. The mCT TOF resolution of 580ps [9] allowed for a constant bed motion speed of 4.2mm/sec, which is count-equivalent to an SS bed frame of 30sec.

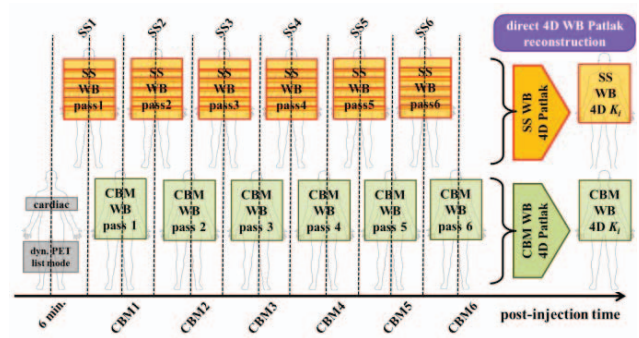


Fig. 4: Dynamic WB PET acquisition protocol employed for the objective evaluation of the clinical performance of the proposed CBM-based versus the conventional SS-based direct 4D WB Patlak reconstruction algorithm.

## III. Results and Discussion

In Fig. 5 we present the series of WB dynamic 18F-FDG PET clinical images, as reconstructed from the temporally interleaved 6 SS (1st row) and 6 CBM (2nd row) passes. A visual inspection of the high uptake foci, which is located in a bed overlap region, suggests superior target-to-background ratio (TBR) for the CBM WB PET SUV images.

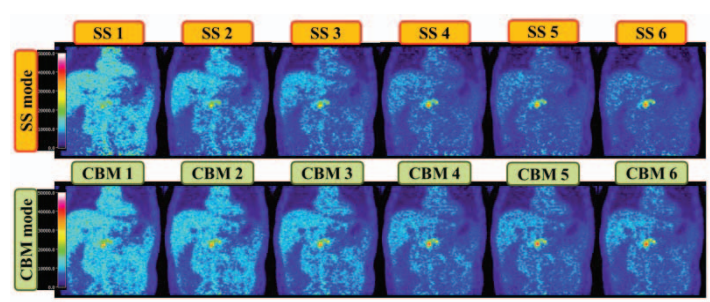


Fig. 5: The series of the dynamic WB 18F-FDG PET images reconstructed from the respective WB SS (1st row) and CBM (2nd row) passes.

Furthermore, the data from the last 3 WB passes of each mode were added together to produce synthetic sinogram PET data that can be considered noise-equivalent to static PET sinograms of the same total scan duration. The synthesized sinograms were then reconstructed with Ordinary Poisson (OP) OS-EM (3 iterations, 21 subsets) to produce the WB PET images in Fig. 6, which may also be considered as noise-equivalent to static PET images.

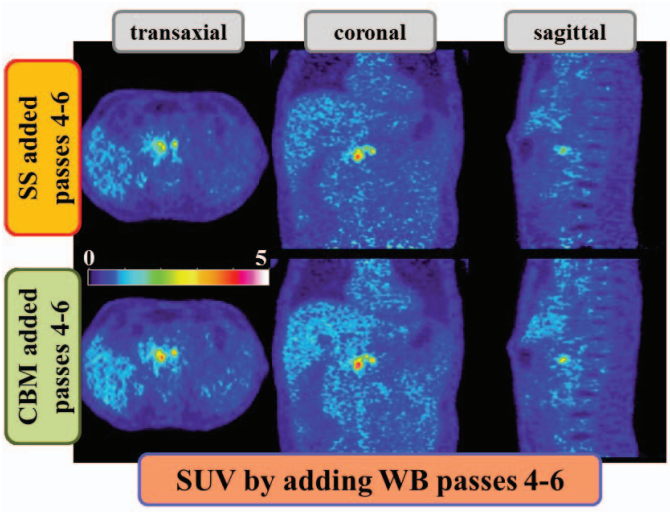


Fig. 6: Static WB 18F-FDG SUV PET images reconstructed with ordinary Poisson (OP) OS-EM algorithm (3 iterations, 21 subsets) from synthesized sinograms, after adding the last 3 passes (i.e. WB passes 4th-6th) of SS (1st row) and CBM (2nd row) acquisition data.

In addition, Fig. 7 presents the WB $K_i$ images, as produced from all six dynamic SS and CBM datasets using the nested 4D SS (1st row) and CBM (2nd row) standard Patlak (sPatlak) OS-EM algorithms respectively (3 global iterations, 21 subsets, 20 nested sPatlak subiterations). The analysis on the identified foci in sPatlak $K_i$ images demonstrated an increase of 40-50% for $K_i$ in the target foci region-of-interest (ROI) and 35-45% for the respective target-to-background ratio (TBR) metric for the CBM relative to SS 4D sPatlak reconstruction.

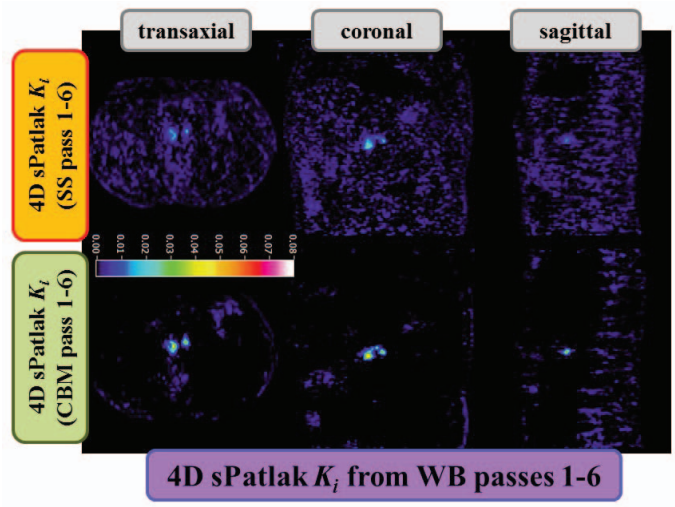


Fig. 7: Standard Patlak (sPatlak) slope ($K_i$) WB 18F-FDG parametric images reconstructed with nested direct 4D sPatlak algorithm (3 global iterations, 20 nested sub-iterations, 21 subsets) employing all dynamic sinograms (i.e. WB passes 1st–6th) of SS (1st row) and CBM (2nd row) acquisition data.

Furthermore, Fig. 8 shows equivalent WB parametric generalized Patlak (gPatlak) $K_i$ image results between the SS (1st row) and CBM (2nd row) scan modes using all acquired WB passes (six for each mode). The final $K_i$ images were reconstructed using 3 total global iterations of the nested gPatlak SS and CBM 4D OS-EM algorithms of which the first two were actually sPatlak iterations to initialize the third gPatlak iteration. Each of the three global iterations included 20 nested sub-iterations. A visual inspection of the reconstructed WB $K_i$ images demonstrated a significant improvement for gPatlak reconstruction with CBM mode. Quantitative ROI analysis in gPatlak $K_i$ images demonstrated a similar TBR performance enhancement as with sPatlak $K_i$ imaging. In particular, gPatlak $K_i$ in the target foci ROI increased by ~50% in target, while the respective TBR scores by ~45% for the CBM relative to the SS 4D gPatlak method.

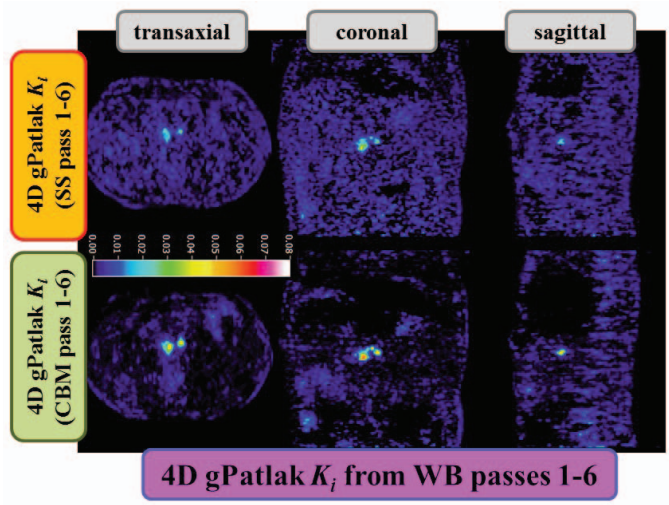


Fig. 8: Generalized Patlak (gPatlak) slope ($K_i$) WB 18F-FDG parametric images reconstructed with nested direct 4D gPatlak algorithm (3 global iterations of which the first 2 were initialization sPatlak iterations, 20 nested sub-iterations, 21 subsets) employing all dynamic sinograms (i.e. WB passes 1st–6th) of SS (1st row) and CBM (2nd row) acquisition data.

On the other hand, it should be noted that in a previous study we had observed a considerably smaller improvement in focal uptake contrast with CBM mode, over SS, when comparing their detectability on either static SUV or indirect sPatlak and gPatlak $K_i$ images for the same clinical data and focal uptake ROIs. We attribute the more significant contrast enhancement with CBM mode for the direct 4D $K_i$ imaging to the relatively higher sensitivity of direct 4D reconstruction in any noise non-uniformities across the axial field of view which may in turn cause noise-induced bias in the reconstructed Ki estimates. With CBM mode the axial sensitivity profile becomes uniform across the whole axial FOV, including in regions where SS acquisition is overlapping. This noise uniformity benefit may more efficiently get exploited, in terms of accuracy and contrast, by direct 4D than indirect parametric imaging algorithms, as the former are more susceptible to noise-induced bias.

## IV. Conclusions

In this study, we exploited the unique feature of dynamic WB PET imaging for multiple fast WB PET scan passes within a single exam session to enable a more objective and quantitative comparison between conventional step-and-shoot (SS) and state-of-the-art continuous bed motion (CBM) WB PET acquisition modes. In particular we interleaved the acquisition equally between the two modes using a previously validated and optimized dynamic WB PET/CT imaging protocol and then added the acquired data of the last three WB passes from each mode before reconstructing to directly obtain within the same total scan window perfectly co-registered SS and CBM WB PET clinical images.

In addition, we employed the same set of acquired WB dynamic PET/CT clinical data to design and validate a novel nested direct 4D WB parametric PET image reconstruction method from CBM PET data using either robust sPatlak or more quantitative gPatlak graphical analysis. Furthermore, we objectively compared the clinical performance of our proposed CBM 4D methods against equivalent 4D WB parametric reconstruction algorithms designed for SS WB PET data as well as conventional static SUV imaging.

Our results have demonstrated superior visual contrast and TBR scores in suspected focal uptake regions for both the SS and the CBM 4D sPatlak and gPatlak WB $K_i$ clinical images over conventional static SS or CBM PET SUV respective images. In addition, we observed significantly enhanced visual contrast and TBR scores for both sPatlak and gPatlak 4D WB $K_i$ images when reconstructed from CBM over SS PET data. The same contrast enhancement was relatively smaller for indirect WB $K_i$ imaging, as we had shown in a previous study for the same clinical data. Finally, a similar improvement in contrast is observed for both sPatlak and gPatlak 4D $K_i$ imaging when SS is replaced by CBM scan mode.

Therefore, we have demonstrated in this study that our proposed direct 4D nested slice-wise WB sPatlak and gPatlak reconstruction methods may enhance quantification and lesion detectability by exploiting the noise suppression of 4D algorithms and the uniform axial sensitivity of CBM PET acquisitions. Thus, they can be considered an important complement to currently established in clinic, but semi-quantitative, static WB SUV PET imaging. Currently, we validate novel dynamic WB PET scan protocols that allow for combined SUV and $K_i$ WB PET imaging within the same late scan session that was previously used only for SUV [49]. The novel SUV/Patlak WB PET imaging framework is compatible with SS or CBM scan modes and indirect or direct 4D reconstruction, it supports quantitative 4D gPatlak analysis from late passes, relative to injection [50], and employs population-based input function models to estimate the missing early section of the input function[51,52].

## V. Acknowledgments

The authors would like to gratefully acknowledge support by Siemens Medical Solutions, the Swiss National Science Foundation under Grant SNSF 31003A-149957 and the Swiss Cancer Research Foundation Grant KFS-3855-02-2016.

## References

[1] S. F. Schubert, S. Pajevic and R. E. Carson “Whole body PET using overlapped 3D acquisition and weighted image summation,” IEEE Nucl Sc Symp Med Imag Conf (NSS/MIC), Anaheim, CA, p. 1285-1289, 1996

[2] M. Dahlbom, P.D. Cutler, W.M. Digby, W.K. Luk, and J. Reed, “Characterization of sampling schemes for whole body PET imaging,” IEEE Trans Nucl Sc, 41, p. 1571-1576, 1994

[3] P.D. Cutler and M. Xu, ”Strategies to improve 3D whole-body PET image reconstruction,” Phys Med Biol, 41, p. 1453-1467, 1996

[4] A. Chatziioannou and M. Dahlbom, "Study of the effects of whole body PET spatial sampling schemes on data SNR," IEEE Nucl Sc Symp Med Imag Conf (NSS/MIC), Anaheim, CA, p. 1295-1299, 1996

[5] N. A. Karakatsanis, M. A. Lodge, A. K. Tahari, Y. Zhou, R. L. Wahl and A. Rahmim, “Dynamic whole-body PET parametric imaging: I. Concept, acquisition protocol optimization and clinical application,” Phys Med Biol, 58(20), p. 7391-7418, 2013

[6] N. A. Karakatsanis, M. A. Lodge, Y. Zhou, R. L. Wahl and A. Rahmim, “Dynamic whole-body PET parametric imaging: II. Task-oriented statistical estimation,” Phys. Med. Biol. 58(20), p. 7419-7445, 2013

[7] J. S. Karp, S. Surti, M. E. Daube-Witherspoon and G. Muehllehner, “Benefit of time-of-flight in PET: experimental and clinical results,” J. Nucl. Med., 49(3), p. 462-470, 2008

[8] V. Y. Panin, F. Kehren, C. Michel and M. E. Casey “Fully 3-D PET reconstruction with system matrix derived from point source measurements,” IEEE Trans. in Med. Imag., 25(7), p. 907-921, 2006

[9] B. W. Jakoby, Y. Bercier, M. Conti, M. E. Casey, B. Bendriem and D. W. Townsend, “Physical and clinical performance of the mCT time-of-flight PET/CT scanner,” Phys Med Biol, 56(8), p. 2375-2389, 2011

[10] N. A. Karakatsanis, M. A. Lodge, A. Rahmim, and H. Zaidi, “Introducing Time-of-Flight and Resolution Recovery Image Reconstruction to Clinical Whole-body PET Parametric Imaging,” IEEE Nucl Sc Symp Med Imag Conf (NSS/MIC), Seattle, WA, 2014

[11] A. Rahmim, and J. Tang, “Noise propagation in resolution modeled PET imaging and its impact on detectability,” Phys Med Biol, 58(19), p. 6945-6968, 2013

[12] S. Ashrafinia, N. Karakatsanis, H. Mohy-ud-Din, and A. Rahmim, “Towards continualized task-based resolution modeling in PET imaging. Proc. SPIE Med Imag: Phys Med Imag, 903327, 2014

[13] S. Ashrafinia, H. Mohy-ud-Din, N. A. Karakatsanis, D. J. Kadrmas, and A. Rahmim, “Enhanced quantitative PET imaging utilizing adaptive partial resolution modeling,” J Nucl Med, 55 (suppl. 1), p. 371, 2014

[14] N. A. Karakatsanis, M. A. Lodge, Y. Zhou, J. Mhlanga, M.A. Chaudhry, A.K. Tahari, W.P. Segars, R.L. Wahl and A. Rahmim, 2011, October. Dynamic multi-bed FDG PET imaging: feasibility and optimization. IEEE Nucl Sc Symp Med Imag Conf (NSS/MIC), Valencia, Spain, p. 3863-3870, 2011

[15] S. R. Cherry, M. Dahlbom and E. J. Hoffman, “3D PET using a conventional multislice tomograph without septa,” J Comp Assist Tomogr, 15(4), p. 655-668, 1991

[16] D. W. Townsend, A. Geissbühler, M. Defrise, E. J. Hoffman, T. J. Spinks, D. L. Bailey, M. C. Gilardi, and T. Jones, "Fully three dimensional reconstruction for a PET camera with retractable septa," IEEE Trans Med Imag, MI-10, p. 505-512, 1991

[17] S. Pajevic, M.E. Daube-Witherspoon, S.L. Bacharach, and R.E. Carson, ”Noise characteristics of 3D and 2D PET images,” IEEE Trans Med Imag, 17(1), p. 9-23, 1998

[18] P.E. Kinahan and J.G. Rogers, “Analytic three dimensional image reconstruction using all detected events,” IEEE Trans Nucl Sci, 36, p. 964-968, 1989

[19] S.R. Cherry, M. Dahlbom, and E.J. Hoffman, “Evaluation of a 3D reconstruction algorithm for multi-slice PET scanners,” Phys Med Biol, 37, p. 779-790, 1992

[20] P.E. Kinahan and J.S. Kairp, “Figures of merit for comparing reconstruction algorithms with a volume imaging PET scanner,” Phys Med Biol, 39, p. 63 1-642, 1994

[21] T.K. Lewellen, S.G. Kohlrriyer,R.S. Miyaoka, M.S. Kaplan, C.W. Steams, and S.E Schubert, “Investigation of the performance of the

General Electric Advance positron emission tomograph in 3D mode," IEEE Trans Nucl Sci, 43, p. 2199-2206, 1996

[22] M Dahlbom, D C Yu, S R Cherry, A Chatziioannou and E J Hoffman, "Methods for improving image quality in whole body PET scanning." IEEE Trans Nucl Sc, 39(4), p. 1079-1083, 1992

[23] S. R. Cherry, M. Dahlbom, and E.J. Hoffman, "High sensitivity, total body PET scanning using 3D data acquisition and reconstruction," IEEE Trans Nucl Sci, 39(4), p. 1088-1092, 1992

[24] M. Dahlbom, A. Chatziioannou, and C. K. Hoh, "Resolution characterization of continuous axial sampling in whole body PET," IEEE Nucl Sc Symp Med Imag Conf (NSS/MIC), San Francisco, CA, 1995

[25] M. A. Flower, K. Erlandsson, P. Collins, A. J. Reader, J. R. Symonds-Tayler, L. L. White, and R. J. Ott, "Spiral whole-body PET - Implementation and initial results," J Nucl Med, 40(5), p. 279, 1999

[26] K. Erlandsson, M. A. Flower, P. Collins, A. J. Reader, J. R. N. Symonds-Tayler, L. L. White, and R. J. Ott, R. "Spiral PET for whole-body studies with rotating planar detectors," Proc. Int. Meet Fully 3D Imag Recon Radiol Nucl Med, p. 77-79, 1999

[27] M. Dahlbom, J. Reed, and J. Young, "Implementation of true continuous bed motion in 2-D and 3-D whole-body PET scanning," IEEE Trans Nucl Sc, 48(4), p. 1465-1469, 2001

[28] D. Brasse, D. Newport, J. P. Carney, J. T. Yap, C. Reynolds, J. Reed, J. Bao, P. Luk, C. Michel, and D. W. Townsend, "Continuous bed motion acquisition on a whole body combined PET/CT system," IEEE Nucl Sc Symp Med Imag Conf (NSS/MIC), Norfolk, VA, 2, p. 951-955, 2002

[29] D. W. Townsend, J. Reed, D. F. Newport, J. PJ Carney, S. Tolbert, D. Newby, J. T. Yap, and M. J. Long, "Continuous bed motion acquisition for an LSO PET/CT scanner," IEEE Nucl Sc Symp Med Imag Conf (NSS/MIC), Rome, Italy, 4, p. 2383-2387, 2004

[30] Z. Burbar, C. Michel, D. Towsend, B. Jakoby, M. Sibomana, F. Kehren, S. Tolbert, J. Reed, K. Hubner, and M. Abidi, "Continuous bed motion data processing for a resolution LSO PET/CT scanner.," IEEE Nucl Sc Symp Med Imag Conf (NSS/MIC), Puerto Rico, 4, p. 2046-2048, 2005

[31] D. F. Newport, M. E. Casey, W. K. Luk, and J. H. Reed, "Continuous tomography bed motion data processing apparatus and method," U.S. Patent 6,915,004, July 5, 2005

[32] V. Y. Panin, "Random Sinogram Variance Reduction in Continuous Bed Motion Acquisition," U.S. Patent Application 13/737,437, January 9, 2013

[33] V. Y. Panin, and M. E. Casey, "Normalization Coefficients in PET Continuous Bed Motion Acquisition," U.S. Patent Application 13/739,458, January 11, 2013

[34] V. Y. Panin, A. M. Smith, and M. E. Casey. "Normalization coefficient computing for continuous bed motion acquisition," IEEE Nucl Sc Symp Med Imag Conf (NSS/MIC), Seoul, S. Korea, p. 1-10, 2013

[35] V. Y. Panin, A M Smith, J Hu, F. Kehren and M. E. Casey, "Continuous bed motion on clinical scanner: design, data correction, and reconstruction," Phys Med Biol, 59(20), p. 6153-6174, 2014

[36] N.A. Karakatsanis, V. Garibotto, O. Rager, and H. Zaidi, H "Continuous bed motion vs. step-and-shoot acquisition on clinical whole-body dynamic and parametric PET imaging. IEEE Nucl Sc Symp Med Imag Conf (NSS/MIC), San Diego, CA, p. 1-6, 2015

[37] N. A. Karakatsanis, M. A. Lodge, R. L. Wahl and A. Rahmim, "Direct 4D whole-body PET/CT parametric image reconstruction: concept and comparison vs. indirect parametric imaging," J Nucl Med, 54 (Supplement 2), p. 2133-2133, 2013

[38] N. A. Karakatsanis and A. Rahmim, "Whole-body PET parametric imaging employing direct 4D nested reconstruction and a generalized non-linear Patlak model," Proc. SPIE Med Imag: Phys Med Imag, 90330Y, 2014

[39] W. Zhu, Q. Li, B. Bai, P. S. Conti, and R. M. Leahy, "Patlak image estimation from dual time-point list-mode PET data," IEEE Trans Med Imag 33(4), p. 913-924, 2014

[40] N.A. Karakatsanis, M.E. Casey, M.A. Lodge, A. Rahmim, and H. Zaidi, "Whole-body direct 4D parametric PET imaging employing nested generalized Patlak expectation–maximization reconstruction," Phys. Med. Bio., 61(15), p. 5456-5485, 2016

[41] C. S. Patlak, R. G. Blasberg, and J. D. Fenstermacher, "Graphical evaluation of blood-to-brain transfer constants from multiple-time uptake data," J. Cereb. Blood Flow Metab., 3(1), p. 1-7, 1983

[42] C. S. Patlak and R. G. Blasberg, "Graphical evaluation of blood-to-brain transfer constants from multiple-time uptake data. Generalizations," J. Cereb. Blood Flow Metab., 5, p. 584-590, 1985

[43] N. A. Karakatsanis, Y. Zhou, M. A. Lodge, M. E. Casey, R. L. Wahl, H. Zaidi and A. Rahmim, "Quantitative whole-body parametric PET imaging incorporating a generalized Patlak model," IEEE Nucl Sc Symp Med Imag Conf (NSS/MIC), p. 1-9, 2013

[44] N. A. Karakatsanis, Y. Zhou, M. A. Lodge, M. E. Casey, R. L. Wahl, H. Zaidi and A. Rahmim "Generalized whole-body Patlak parametric imaging for enhanced quantification in clinical PET," Phys Med Biol, 60(22), p. 8643-8673, 2015

[45] G. Wang, and J. Qi, "Acceleration of the direct reconstruction of linear parametric images using nested algorithms," Phys Med Biol, 55(5), p. 1505-1517, 2010

[46] N.A. Karakatsanis, H. Zaidi, and C. Tsoumpas, "Generalized 3D and 4D motion compensated whole-body PET image reconstruction employing nested EM deconvolution," IEEE Intern. Conf. Imaging Syst. Tech. p. 263-268, 2014

[47] N.A. Karakatsanis, C. Tsoumpas, and H. Zaidi, "Quantitative PET image reconstruction employing nested expectation-maximization deconvolution for motion compensation," Comp. Med. Imaging Graph., (in press), 2016

[48] D R Osborne, S Acuff, S. Cruise, M. Syed, M. Neveu, A. Stuckey and Y. Bradley "Quantitative and qualitative comparison of continuous bed motion and traditional step and shoot PET/CT," Am J Nucl Med Mol Imag, 5(1), p. 56-64, 2015

[49] N. A. Karakatsanis, M. Lodge, Y. Zhou, M. Casey, R. Wahl, R. Subramaniam, H. Zaidi, and A. Rahmim, "Novel multi-parametric SUV/Patlak FDG-PET whole-body imaging framework for routine application to clinical oncology," J Nucl Med, 56 (Supplement 3), p. 625-625, 2015

[50] N. A. Karakatsanis, M. A. Lodge, M. E. Casey, H. Zaidi and A. Rahmim, "Impact of Acquisition Time-Window on Clinical Whole-Body PET Parametric Imaging," IEEE Nucl Sc Symp Med Imag Conf (NSS/MIC), 2014

[51] Y. Zhou, S. Zhang, J. Zhang, N. Karakatsanis, A. Rahmim, M. Lodge, R. Wahl, D. Wong, and R. F. Wang, "Generalized population-based input function estimation given incomplete blood sampling in quantitative dynamic FDG PET studies," J Nucl Med, 53 (Supplement 1), p. 380-380, 2012

[52] N. Karakatsanis, Y. Zhou, M. Lodge, M. Casey, R. Wahl, R. Subramaniam, A. Rahmim, and H. Zaidi, "Clinical Whole-body PET Patlak imaging 60-90min post-injection employing a population-based input function," J Nucl Med 56, (Supplement 3), p. 1786-1786, 2015